Channel fringes in PFM1 High Resolution Interferograms

David Naylor, Trevor Fulton, Peter Davis
11 April 2005

1 Introduction

The purpose of this document is to present the first results of the analysis of the channel fringes observed in the high-resolution interferograms data taken during the SPIRE PFM1 test campaign. The location of these features is quantified, potential candidates for their cause presented, and solutions for their removal/minimization proposed.

2 Background

Most of the high-resolution interferograms observed during the PFM1 test campaign exhibit channel fringes – coherent signatures at increased OPDs resulting from resonant cavities within the optical path of the interferometer (Naylor *et. al.*[1]). Figure 1 shows an interferogram of SLW observed on 08 March, with the cold blackbody (T = 6K) as a source in one port the SPIRE FTS and the interior of the cryostat (SCAL switched off) in the other port. Note the dominant feature present from about 9 to 11 cm OPD for SLW. It is this feature that is the subject of this note.

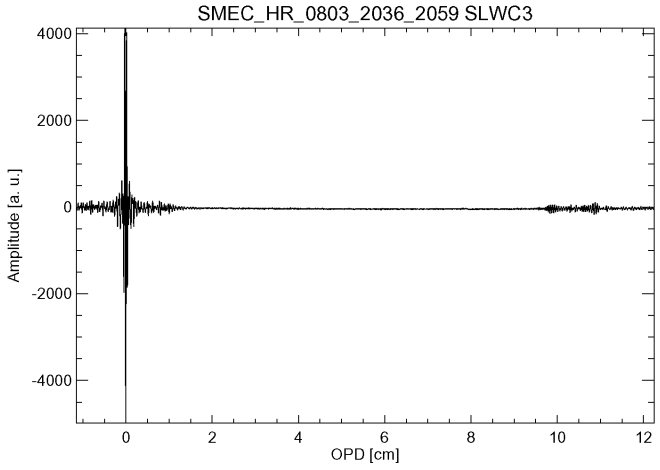

Figure 1: Typical high-resolution SLW interferogram observed during the SPIRE PFM1 test campaign

[1] D. A. Naylor, A. A. Schultz and T. A. Clark, "Eliminating channel spectra in Fourier transform spectroscopy", Appl. Opt., **27**, 2603 (1988)

Figure 2 shows the same interferogram, but with two regions highlighted. The region coloured green is a 1024-point window centred at the zero path difference position. The region highlighted in red is a 1024-point window of the channel fringe.

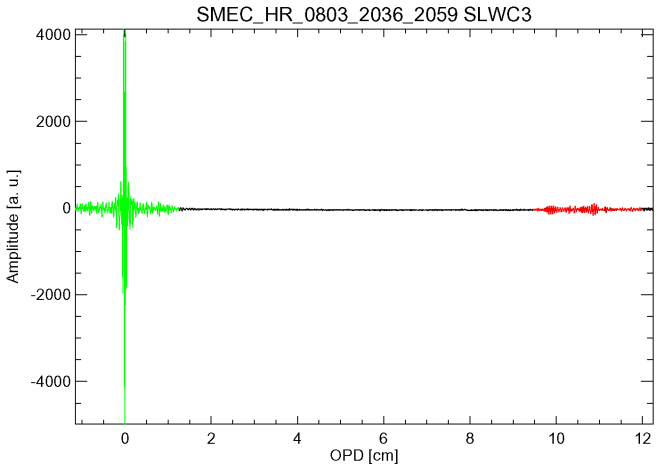

Figure 2: SPIRE PFM1 SLW interferogram. The green portion is the region about zero path difference, the red portion is a region containing the channel fringe.

Figures 3 and 4 show the power spectra for the green and red regions of the interferogram. The first figure shows the entire spectrum up to the Nyquist frequency, while the second figure shows only that portion of the spectrum within the SLW band. Note that in each of these figures the power spectrum for the red region has been scaled so that its maximum agrees with the maximum of the power spectrum of the green region.

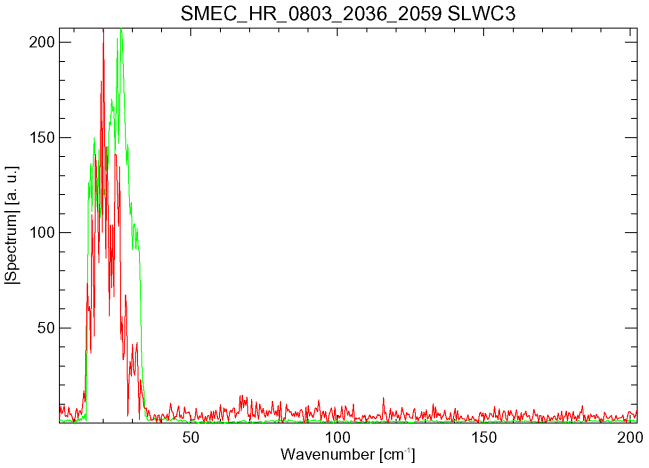

Figure 3: SPIRE PFM1 SLW spectrum. The green curve is the power spectrum from the ZPD portion of the interferogram, the red curve is the power spectrum from that portion of the

interferogram containing the channel fringe. The red curve has been scaled to match the green curve.

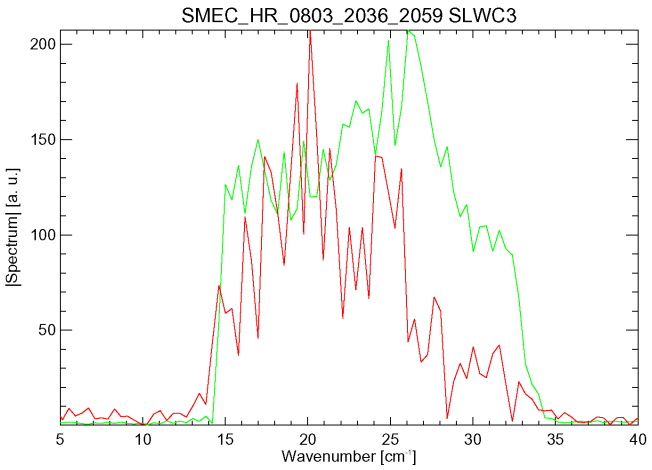

Figure 4: expanded region of Figure 3.

Figure 4 clearly shows that the channel fringe contains essentially the same spectral components as those derived from the ZPD information.

The above analysis was undertaken for all of the pixels in both the SLW and SSW arrays for all of the cold blackbody observations taken on 08 March 2005. The figures that follow show some sample interferograms for all of the SLW and SSW pixels for the 11K and 13K cold blackbody observations. For each plot, only that portion of the interferogram that contains the channel fringe is shown. The channel fringe is present in most of the detector pixels in both arrays, the notable exceptions being SSWD5, SSWD7, SSWF4, SSWG3, and SSWG4 pixels on which very little signal was observed.

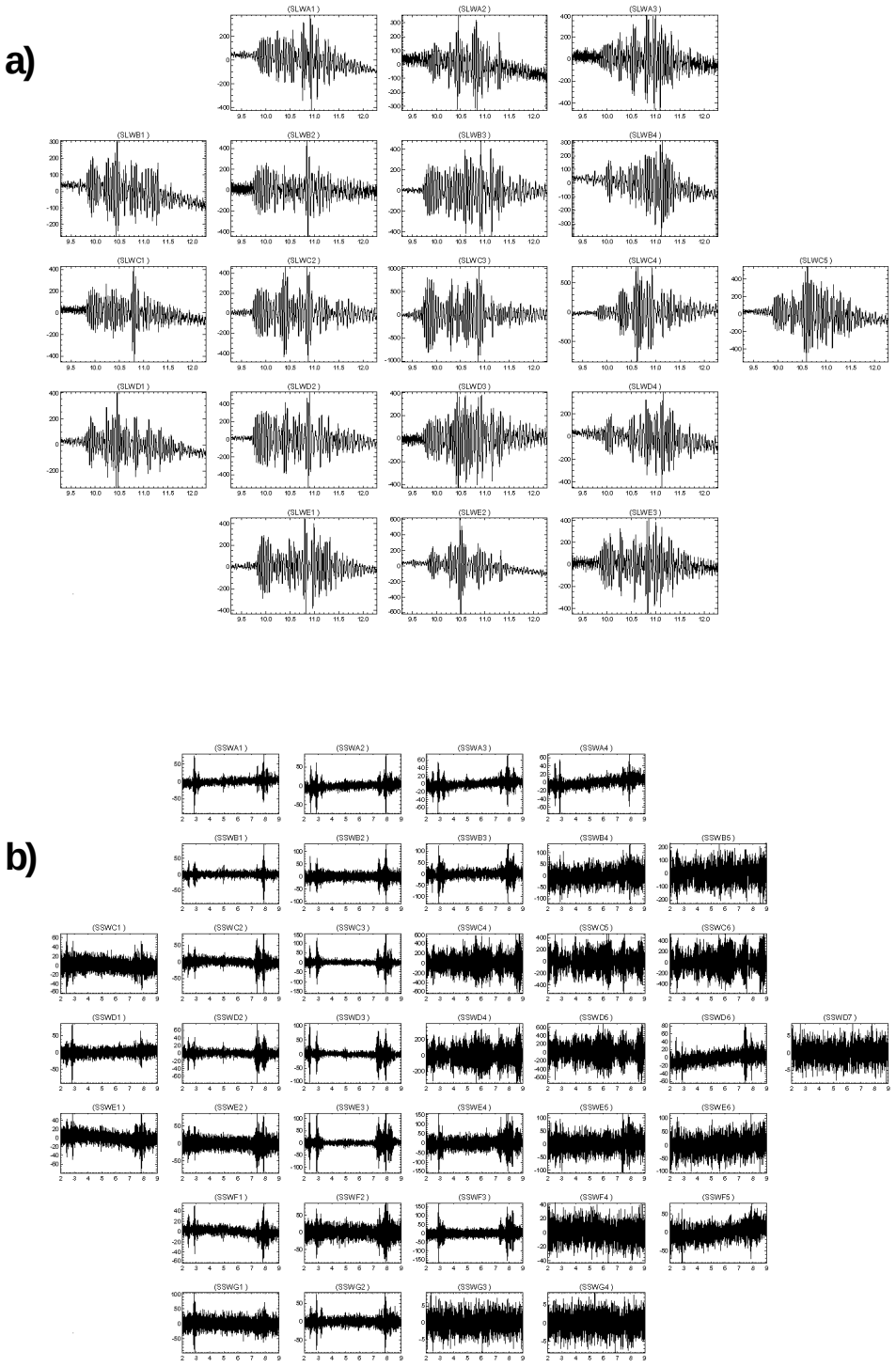

Figure 5: Observed channel fringes a) SLW (labelled range 9.8 – 12 cm opd), b) SSW (labelled range 2 – 9 cm opd)

Figures 6-9 show a more detailed analysis of the channel fringes for two pixels in each array when the cold blackbody was set to 11K. The pixels featured are SLWA1, SLWC3, SSWA2, and SSWD3. In each figure, a sample raw interferogram is shown in the upper left plot; the corresponding baseline corrected interferogram is shown in the upper right plot. The two plots in the middle show a close-up view of the ZPD region on the left and a close-up view of the region containing the channel fringe on the right. The two plots on the bottom show the spectra for both of the interferogram regions; the black curve is the spectrum of the ZPD region while the red curve is the spectrum of the channel fringe (scaled by a factor of 10).

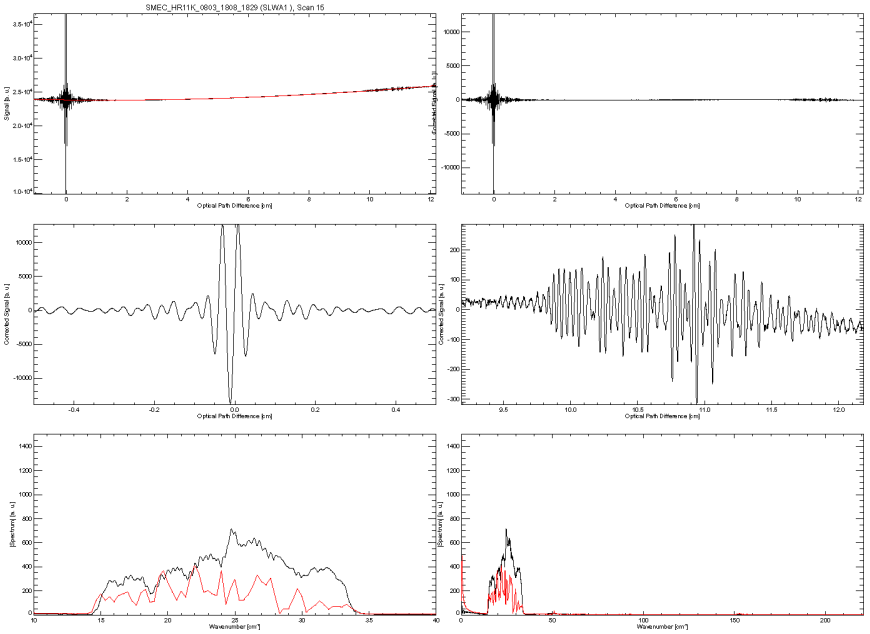

Figure 6: Channel fringe analysis: pixel SLWA1. Labelled ranges: Top 0 – 12 cm opd; middle - 0.5 – 0.5 cm opd and 9.8 – 12 cm respectively.

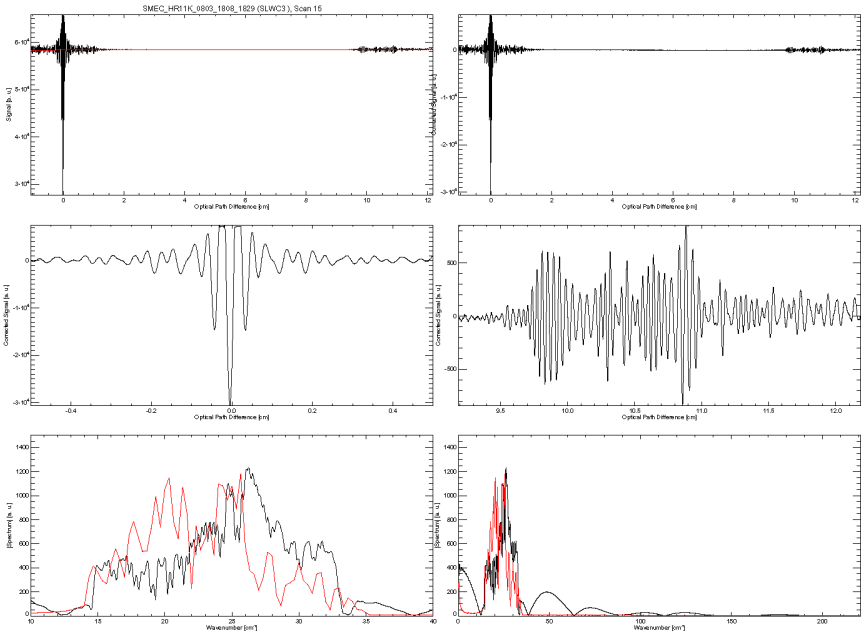

Figure 7: Channel fringe analysis: pixel SSWC3. Labelled ranges: Top 0 – 12 cm opd; middle - 0.5 – 0.5 cm opd and 9.8 – 12 cm respectively.

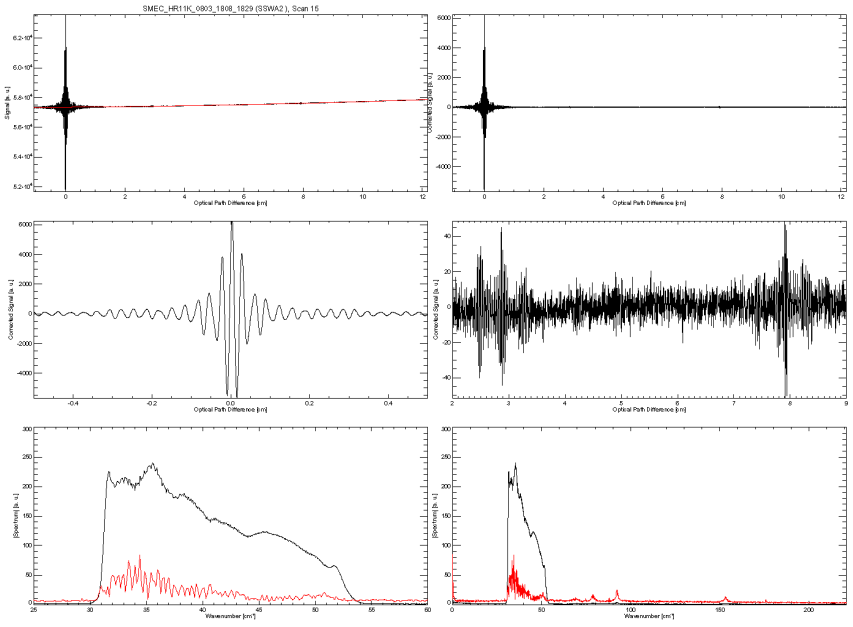

Figure 8: Channel fringe analysis: pixel SSWA2. Labelled ranges: Top 0 – 12 cm opd; middle - 0.5 – 0.5 cm opd and 2 – 9 cm respectively.

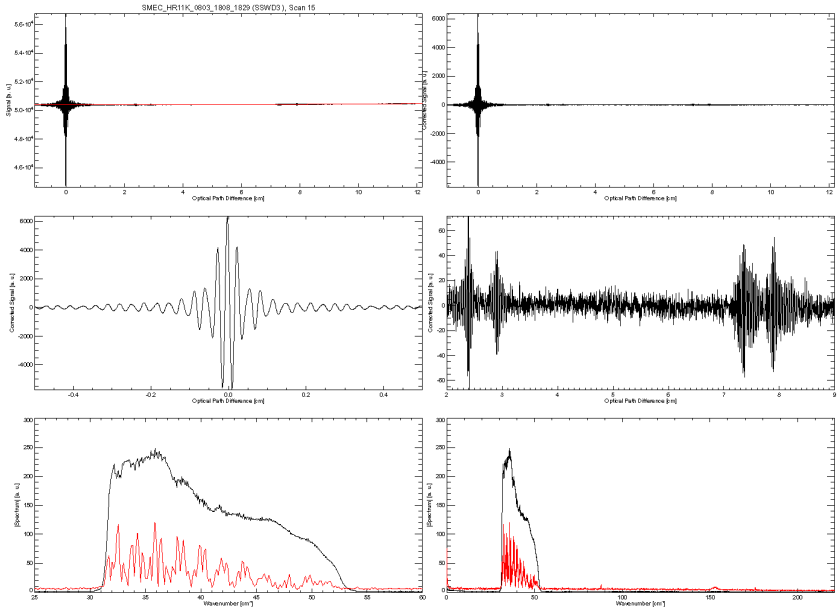

Figure 9: Channel fringe analysis: pixel SSWD3 Labelled ranges: Top 0 – 12 cm opd; middle - 0.5 – 0.5 cm opd and 2 – 9 cm respectively.

Figures 6 – 9 show that channel fringes appear on both the central pixels (SLWC3 and SSWD3) as well as the outer pixels (SLWA1 and SSWA2). Moreover, as observed previously, the spectral content of the channel fringe lcontains essentially the same spectral components as those derived from the ZPD information. Moreover, while the location of the channel fringes are similar for pixels of the same array, there is a marked difference in the location of the features between the two detector arrays.

3 Quantitative Analysis

An analysis was undertaken in order to determine the location of the channel fringes observed in the high-resolution interferograms. Although the location of the fringes is similar from one pixel to another of the saem array, their shape changes which makes it difficult to pinpoint the exact location of the feature. In light of this, it was decided to concentrate in this preliminary analysis on two aspects of the channel fringes; the location of the onset of the fringe and the location of the maximum deviation from the baseline within the fringe. These two positions were found for each of the pixels in both arrays. The procedure employed to determine these position is described below:

1. The recorded detector signals were interpolated onto an evenly spaced position grid (using the interpolated SMEC positions) to create an interferogram.
2. The interferograms were then divided into sub-regions according to the presence of the channel fringe. For the SLW array the sub-region was from 9cm to 13cm OPD. For the SSW array, two sub-regions were used; the first was from 1.8 to 4.0 cm OPD, the second was of the range between 6.6 and 8.6 cm OPD.
3. In order to increase the signal to noise ratio of the interferograms, a series of interferograms were averaged together. Due to the inherent asymmetries between the forward and reverse interferograms forward and reverse scans were averaged independently.
4. Within each of the subsections, the position where the maximum deviation from the baseline signal was recorded. To determine the position where the signal first starts to deviate from the baseline, the so-called onset of the fringe, a threshold equal to a fraction of the maximum deviation within the region of interest was used. The onset positions were calculated for a series of fractional values and then averaged together. (Trevor used a range of fractional values for the determination of the onset of the fringing were 20%, 25%, 30%, 35%, 40%, 45%, and 50%.)

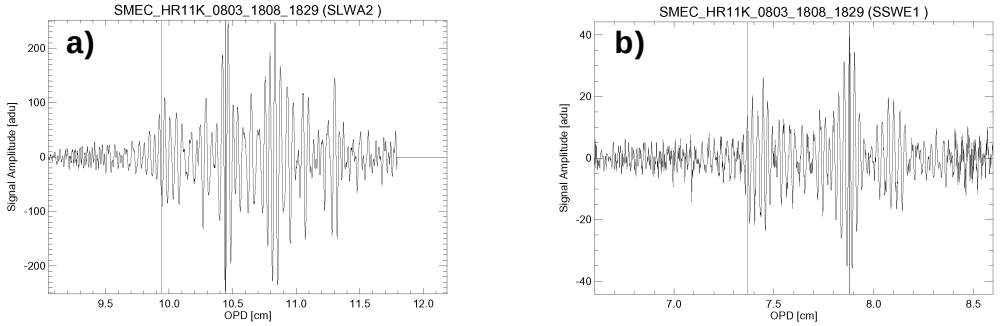

Figure 10: Channel fringe regions a) SLW, b) SSW. The green lines show the positions of the onset of the fringe feature, the red lines show the positions of maximum deviation within the feature region. For these figures, a threshold of 35% of the maximum deviation was used to determine the onset of the channel fringe.

Based on the above criteria, the positions of the onset and the maximum deviation for the recognizable channel fringes were determined and are shown in the following tables. Note that the entries in red denote those pixels in the SSW array that were observed to have higher noise levels.

Pixel	A	B	C	D	E
1	10.014 ± 0.158	9.876 ± 0.033	9.968 ± 0.171	9.885 ± 0.021	9.872 ± 0.027
2	10.032 ± 0.179	9.878 ± 0.280	9.872 ± 0.201	9.800 ± 0.046	10.082 ± 0.212
3	10.162 ± 0.164	9.833 ± 0.125	9.754 ± 0.020	9.920 ± 0.186	9.925 ± 0.057
4		10.217 ± 0.321	10.312 ± 0.109	10.188 ± 0.281	
5			10.134 ± 0.230		

Table 1: Channel fringe onset locations (cm OPD) for the SLW array, CBB temperature = 11K

Pixel	A	B	C	D	E	F	G
1	2.765 ± 0.228	2.271 ± 0.206	2.134 ± 0.293	2.519 ± 0.286	2.082 ± 0.282	2.287 ± 0.236	2.450 ± 0.499
2	2.296 ± 0.249	2.139 ± 0.288	1.965 ± 0.186	2.116 ± 0.246	1.868 ± 0.102	2.224 ± 0.475	2.410 ± 0.283
3	2.272 ± 0.277	2.239 ± 0.264	2.285 ± 0.206	2.304 ± 0.076	2.332 ± 0.030	2.763 ± 0.274	1.805 ± 0.005
4	2.453 ± 0.084	1.863 ± 0.145	1.808 ± 0.008	1.850 ± 0.150	2.270 ± 0.277	1.827 ± 0.025	1.805 ± 0.008
5		1.818 ± 0.022	1.806 ± 0.006	1.806 ± 0.005	1.893 ± 0.186	2.099 ± 0.357	
6			1.807 ± 0.009	2.026 ± 0.201	1.810 ± 0.012		
7				1.808 ± 0.011			

Table 2: Channel fringe onset locations (cm OPD) for the SSW array, Region = 1.8cm - 4.0cm, CBB temperature = 11K

Pixel	A	B	C	D	E	F	G
1	7.362 ± 0.124	7.707 ± 0.240	7.126 ± 0.299	7.065 ± 0.261	7.259 ± 0.201	7.322 ± 0.203	6.918 ± 0.334
2	7.462 ± 0.231	7.367 ± 0.031	7.286 ± 0.065	7.248 ± 0.092	7.239 ± 0.123	7.093 ± 0.355	7.544 ± 0.250
3	7.477 ± 0.173	7.702 ± 0.178	7.403 ± 0.217	7.221 ± 0.031	7.266 ± 0.043	7.467 ± 0.187	6.617 ± 0.027
4	7.329 ± 0.370	7.088 ± 0.362	6.694 ± 0.204	6.632 ± 0.021	7.183 ± 0.210	6.601 ± 0.000	6.607 ± 0.007
5		6.601 ± 0.000	6.609 ± 0.005	6.610 ± 0.005	6.994 ± 0.370	6.817 ± 0.291	
6			6.610 ± 0.006	7.264 ± 0.235	6.602 ± 0.001		
7				6.607 ± 0.012			

Table 3: Channel fringe onset locations (cm OPD) for the SSW array, Region = 6.6cm - 8.6cm, CBB temperature = 11K

Pixel	A	B	C	D	E
1	10.946	10.458	10.806	10.459	10.809
2	10.450	10.864	10.880	10.885	10.510
3	10.978	10.925	10.865	10.455	10.848
4		11.124	10.628	11.134	
5			10.600		

Table 4: Positions of maximum deviation (cm OPD) for the SLW array, CBB temperature = 11K

Pixel	A	B	C	D	E	F	G
1	2.878	2.473	2.459	2.847	2.879	2.896	2.865
2	2.877	2.908	2.912	2.886	2.662	2.903	2.896
3	2.881	2.908	2.922	2.396	2.395	2.912	2.423
4	2.877	2.875	2.840	2.395	2.931	2.195	2.802
5		2.379	2.606	2.385	2.930	2.865	
6			2.378	2.463	2.475		
7				2.744			

Table 5: Positions of maximum deviation (cm OPD) for the SSW array, Region = 1.8cm - 4.0cm, CBB temperature = 11K

Pixel	A	B	C	D	E	F	G
1	7.902	7.903	7.884	7.817	7.881	7.902	7.906
2	7.924	7.929	7.897	7.421	7.874	7.889	7.865
3	7.915	7.924	7.899	7.902	7.902	7.884	7.394
4	7.897	7.934	7.937	7.942	7.888	6.895	7.141
5		7.937	7.500	8.352	7.652	7.829	
6			8.037	7.429	7.939		
7				7.622			

Table 6: Positions of maximum deviation (cm OPD) for the SSW array, Region = 6.6cm - 8.6cm, CBB temperature = 11K

4 Possible causes of channel fringe features

Naylor *et. al.* have shown that channel fringes like the ones observed in the SPIRE PFM1 high-resolution interferograms can be attributed to a resonant cavity located in, and normal to, the parallel output beam. The channel fringes appear at positions of optical path difference, ?, given by

$$\Delta = \pm 2mnd \qquad (m = 1,2,3,\ldots,\infty) \qquad \textbf{(1)}$$

where n is the refractive index of the sample and d is the cavity thickness at normal incidence.

The optical layout of SPIRE shows that while there are no cavities in the output beam that are plane-parallel, the field lenses located at the entrance to the SLW and SSW detector assemblies have the potential to set up a resonant cavitiy at these long wavelengths. The field lens alone cannot be responsible for the observed features since they occur at different opds for the two wavebands. However, resonant cavities formed with the field lens do provide an explanation of the observed fringes (see Figure 11).

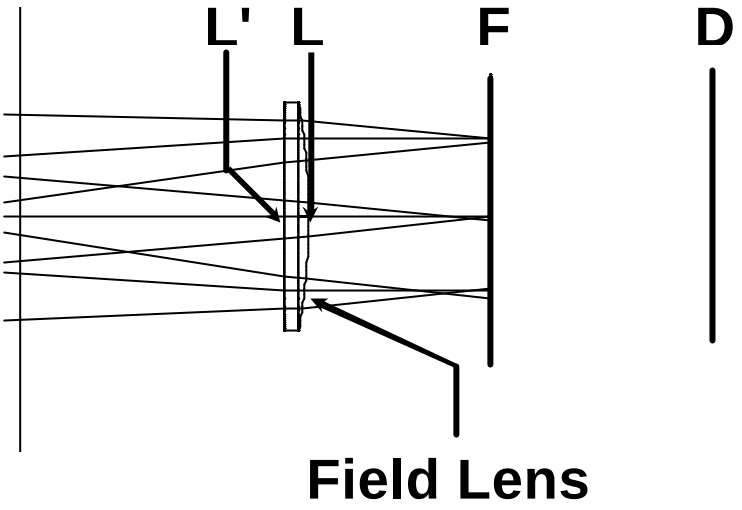

Figure 11: Spectrometer lens -- filter -- detector schematic diagram.[2]

The following tables provide a description of the labels in Figure 11 as well as the distances[3] between selected locations for each BDA.

Label	Description
L'	Flat Surface of Field Lens
L	Powered Surface of Field Lens
F	Geometrical Focal Plane (Feed horn entrance)
D	Detector Plane

Table 7: Description of labels in Figure 11.

Description	Label	Distance [mm]	
		SLW	SSW
Powered Lens Surface to Focal Plane	LF	1.71	11.91
Flat Lens Surface to Focal Plane	L'F	3.35	13.55
Powered Lens Surface to Detector Plane	LD	48.07	35.59
Flat Lens Surface to Detector Plane	L'D	49.71	37.23

Table 8: Distances between selected points for each BDA assembly.

[2] B. M. Swinyard, K. Dohlen, D. Ferand, J.-P. Baluteau, D. Pouliquen, P. Dargent, G. Michel, J. Martignac, P. Ade, P. Hargrave, M. Griffin, D. Jennings, and M. Caldwell, "The Imaging FTS for Herschel SPIRE", SPIRE-RAL-PUB-001696

[3] Hargrave, P and Tucker, C, "EIDP SPIRE - 300mK Spectrometer Filters – PFM", Issue 1.1, 28 November 2003

Table 9 shows the theoretical channel fringe locations based on the dimensions given in Table 8 and Equation 1.

Array	Reflecting Surfaces	Label	Fringe Location (cm OPD)	
			Central Pixel	Edge Pixel
SLW	Powered Lens Surface and Detector Plane	LD	9.653	9.781
	Flat Lens Surface and Detector Plane	L'D	10.169	10.096
SSW	Powered Lens Surface and Focal Plane	LF	2.382	2.510
	Flat Lens Surface and Focal Plane	L'F	2.541	2.825
SSW	Powered Lens Surface and Detector Plane	LD	7.146	7.274
	Flat Lens Surface and Detector Plane	L'D	7.304	7.589

Table 9: Expected channel fringe positions for the SLW and SSW arrays based on reflections from the field lens.

Note that for the SLW array, only the reflection between the detector plane and the field lens (L'D, LD) is considered since the theoretical location for the reflection between the focal plane and the field lens (L'F, LF) gives a theoretical fringe location very close to the zpd position. Such a fringe is very difficult to separate from the heavily modulated signal near ZPD. Table 10 presents a comparison between the expected and observed channel fringe locations.

Array	Reflecting Surfaces		Fringe Location (cm OPD)		
			Expected	Observed	
				Onset	Maximum Deviation
SLW	Powered Lens Surface and Detector Plane	min	9.653	9.75	10.46
	Flat Lens Surface and Detector Plane	max	10.169	10.31	11.13
SSW	Powered Lens Surface and Focal Plane	min	2.382	2.03	2.46
	Flat Lens Surface and Focal Plane	max	2.825	2.76	2.92
SSW	Powered Lens Surface and Detector Plane	min	7.146	7.07	7.43
	Flat Lens Surface and Detector Plane	max	7.589	7.47	7.93

Table 10: Comparison between expected and observed channel fringe locations for the SLW and SSW arrays.

Table 10 strongly suggests that the interference arising from reflections between both surfaces of the field lens and the front and back of the detector assembly is the most likely cause of the channel fringes observed in the SPIRE PFM1 data. The fact that the fringes are not direct copies of the zpd signal is simply due to the convex surface of the field lens which introduces a path difference variation with angle. It can be seen from Table 1 that the onset position is of the channel fringe is least for the central pixel and increases for off axis pixels as would be expected with an increasing gap in the resonant cavity. It is somewhat surprising that the most intense fringe appears to be due to a reflection from the plane of the detectors and not the focal plane.

5 Possible remedies

Since there would appear to be compelling evidence for the field lenses being the principle source of the channel fringes possible remedies include:

1. Remove the field lenses and live with the non-telecenticity of the beam. (Filter may still set up a resonant cavity)
2. Use lower refractive index lenses or better still antireflection coat the lenses (on both surfaces) Peter Ade's group has made significant advances in this area in recent years and this will certainly help.
3. Reverse (ar-coated) lens orientation – this would give greater fringe amplitude (more parallel cavity) but less cross talk (from radiation entering neighbouring horns). Our experience (Naylor et al.) has been that it is easier to correct for a channel fringe formed by a parallel cavity. (The devil you know being better than the one you don't!)
4. Redesign/rebuild detector feedhorn assembly to have spherical integrating cavities – clearly an unacceptable option.

If the analysis is correct, it is somewhat surprising that significant energy is returned from the detector block to the field lens where, having reflected off the convex surface, it can enter an adjacent feedhorn. Cross talk is one aspect of the PFM1 tests that is difficult to measure but must surely be occurring. Unfortunately the fact that one end of the cavity has a convex surface makes it very difficult to estimate the absolute magnitude of the channel fringe.

Note: while it may seem that a simple solution would be to measure interferograms out to opds just less than the location of the channel fringe, one must remember, however, that this is a coherent pattern with information contained at all opds. Moreover, since there will be no simple relation between the phase of the zpd region and that of the channel fringe, detailed phase correction will prove difficult – especially in the case of SLW where, if the analysis is correct, a channel fringe must exist close to the zpd region.